MgxMn(1–x)(BH4)2 (x = 0-0.8), a cation solid solution in a bimetallic borohydride

Radovan Cerny, Nicolas Penin, Vincenza d'Anna, Hans Hagemann, Etienne Durand, Jakub Ruzicka

$Mg_xMn_{(1-x)}(BH_4)_2$ (x = 0–0.8), a cation solid solution in a bimetallic borohydride

Radovan Černý[a], Nicolas Penin[a, b], Vincenza D'Anna[c], Hans Hagemann[c], Etienne Durand[b], Jakub Růžička[d]

[a] *Laboratory of Crystallography, University of Geneva, 1211 Geneva, Switzerland*
[b] *CNRS, Université de Bordeaux 1, ICMCB, 87 Avenue du Docteur Albert Schweitzer, F-33608 Pessac Cedex, France*
[c] *Department of Physical Chemistry, University of Geneva, 1211 Geneva, Switzerland*
[d] *Charles University, Faculty of Science, Department of Inorganic Chemistry, Hlavova 2030, 128 40, Prague 2, Czech Republic*

Abstract :

A solid solution of magnesium and manganese borohydrides was studied by in situ synchrotron radiation X-ray powder diffraction and infrared spectroscopy. A combination of thermogravimetry, mass and infrared spectroscopy, and atomic emission spectroscopy were applied to clarify the thermal gas desorption of pure $Mn(BH_4)_2$ and a solid solution of composition $Mg_{0.5}Mn_{0.5}(BH_4)_2$. $Mg_xMn_{(1-x)}(BH_4)_2$ (x = 0–0.8) conserves the trigonal structure of $Mn(BH_4)_2$ at room temperature. Manganese is dissolved in the hexagonal structure of α-$Mg(BH_4)_2$, with the upper solubility limit not exceeding 10 mol.% at room temperature. There exists a two-phase region of trigonal and hexagonal borohydrides within the compositional range x = 0.8–0.9 at room temperature. Infrared spectra show splitting of various vibrational modes, indicating the presence of two cations in the trigonal $Mg_xMn_{(1-x)}(BH_4)_2$ solid solutions, as well as the appearance of a second phase, hexagonal α-$Mg(BH_4)_2$, at higher magnesium contents. All vibrational frequencies are shifted to higher values with increasing magnesium content. The decomposition temperature of the trigonal $Mg_xMn_{(1-x)}(BH_4)_2$ (x = 0–0.8) does not vary significantly as a function of the magnesium content (433–453 K). The desorbed gas contains mostly hydrogen and 3–7.5 mol.% diborane B_2H_6, as determined from analyses of the $Mn(BH_4)_2$ and $Mg_{0.5}Mn_{0.5}(BH_4)_2$ samples. An eutectic relation between α-$Mg(BH_4)_2$ and $LiBH_4$ is observed. The solid solution $Mg_xMn_{(1-x)}(BH_4)_2$ is a promising material for hydrogen storage as it decomposes at a similar temperature to $Mn(BH_4)_2$, i.e. at a much lower temperature than pure $Mg(BH_4)_2$ without significantly losing hydrogen weight capacity thanks to substitution of Mn by Mg up to 80 mol.%. The questions of diborane release and reversibility remain to be addressed.

1. Introduction

Metal borohydrides (more precisely tetrahydroborates) are considered possible hydrogen storage materials for mobile applications [1,2]. Borohydrides of alkaline and alkaline earth metals often contain large quantities of hydrogen, e.g. 18.4 wt.% in $LiBH_4$, although the decomposition temperatures are usually high [3]. On the other hand, most of the known transition metal borohydrides, especially those of 3*d* metals, are unstable under ambient conditions [3]. The thermal stability of binary metal hydrides has been found to be inversely related to the metal electronegativity (and thus to the standard redox potential) [3]. A similar relationship was postulated for borohydrides half a century ago [4], and was recently investigated theoretically as well as experimentally [5–7]. Tuning the thermodynamic properties of borohydride-based hydrogen storage materials

* Corresponding author. Tel.: +41 22 379 6450; fax: +41 22 379 6108.
E-mail address: radovan.cerny@unige.ch (R. Černý).

by means of synthesizing bimetallic (alkaline or alkaline earth and transition metal) compounds has been suggested [7]. A similar approach has already been successfully applied to $LiNH_2$ [8,9].

The structural diversity and crystal chemistry of homoleptic metal borohydrides were recently reviewed [10,11], and their hydrogen storage properties have also been addressed [1–3,12]. Several bimetallic borohydrides based on alkaline and alkaline earth metal *A* and on 3*d* transition metal *M* with the general formula $A^{m+}M^{n+}(BH_4)_{m+n}$ have been reported in the literature to date [13–15], though implying tentative compositions. In addition to this a DFT calculation based screening of bimetallic borohydrides has also been attempted [16]. However, only recently the crystal structures of $LiSc(BH_4)_4$ [17], $NaSc(BH_4)_4$ [18], $KSc(BH_4)_4$ [19], $LiZn_2(BH_4)_5$, $NaZn_2(BH_4)_5$, $NaZn(BH_4)_3$ [20], $Li_4Al_3(BH_4)_{13}$ [21] and $NaAl(BH_4)_4$ [22] were determined.

Mixing between $[BH_4]^{-1}$ and halogen H^{-1} is often observed on the anionic site [18,19,23,24], resulting in fully ordered structures in some cases, e.g. $KZn(BH_4)Cl_2$ [25]. However, substitution on the cationic site in the bimetallic borohydrides has revealed only fully ordered structures so far. A mixed compound $Mg_xZn_{(1-x)}(BH_4)_2$ has been reported [26], but no details were provided of its structure or its desorption properties.

The crystal structure of the room temperature modification of magnesium borohydride, α-$Mg(BH_4)_2$, was first characterized in the hexagonal space group $P6_1$ [27,28], and with the help of DFT optimization [29], corrected to the higher symmetry of $P6_122$ [30] later on. Following this the structure of the first 3*d* metal borohydride, $Mn(BH_4)_2$, was solved in the trigonal space group $P3_112$ [31], and an interesting structural relationship was revealed between the two compounds, as elucidated in Černý et al. [31]. Both structures are built of similar layers stacked along the *c*-axis and rotated against each other by the respective symmetry operations; by 120° for the 3_1 axis in $Mn(BH_4)_2$ and by 60° for the 6_1 axis in α-$Mg(BH_4)_2$. The building blocks and connectivity are virtually identical in both cases, composed of cations within the tetrahedral environment of BH_4 groups, and with an approximately linear anion coordination. Neither structure is densely packed. The results obtained by Raman and infrared spectroscopy confirm the close resemblance between $Mn(BH_4)_2$ and α-$Mg(BH_4)_2$.

Structural analogies between magnesium- and manganese-based compounds are not unusual among minerals such as Mn_2SiO_4 (tephroite) and Mg_2SiO4 (α-olivine). The likeness in building principles of both magnesium and manganese borohydrides, the identical oxidation state of the cations (2^+), and the existence of solid solution series among magnesium and manganese binaries such as $Mg_xMn_{(1-x)}F_2$ [32] and $Mg_xMn_{(1-x)}Te_2$ [33] initiated the idea of a solid solution of both borohydrides. In this study we report on the structure and desorption properties of $Mg_xMn_{(1-x)}(BH_4)_2$ ($x = 0$–0.8).

2. Experimental

2.1. Synthesis

The preparation and manipulation of all samples was performed in an argon-filled glove box equipped with a circulation purifier ($p(O_2, H_2O) < 0.1$ p.p.m.). Anhydrous manganese(II) chloride, $MnCl_2$ (Sigma Aldrich,>99%), magnesium chloride, $MgCl_2$ (Sigma Aldrich, >98%) and lithium borohydride, $LiBH_4$ (Sigma–Aldrich, 95%) were combined in a molar ratio of metal chloride to lithium borohydride of 1:2. In order to investigate the effect of cation substitution the molar fraction of magnesium chloride was altered according to:

$$x\mathrm{MgCl_2} + (1-x)\mathrm{MnCl_2} + 2\mathrm{LiBH_4}(x = 0.5, 0.6, 0.7, 0.8, 0.9 \text{ and } 1.0) \quad (1)$$

The mixtures were ball milled under an inert argon atmosphere in a Fritsch Pulverisette 7 planetary mill. Grinding was performed at 600 r.p.m. in a 25 ml stainless steel bowl sealed with lid with a Viton O-ring and three stainless steel balls with diameters of 10, 12 and 15 mm as the milling medium. The ball/powder mass ratio was fixed at 25:1. To prevent the system from overheating and avoid powder agglomeration on the walls of the grinding bowl [34] milling was stopped every 10 min for a cooling break of 5 min. This two-step process was repeated 35 times.

As a reference sample we used the results obtained on the Mn end member $Mn(BH_4)_2$ as reported in Černý et al. [31], both in terms of powder diffraction and thermal desorption studies.

2.2. Laboratory powder X-ray diffraction analysis (PXD)

Two samples were used for thermal desorption analyses, pure $Mn(BH_4)_2$ and a solid solution with $x = 0.5$ (Eq. (1)). For these compositions, as well as their desorbed products, laboratory powder diffraction data was collected in a PANalytical X'Pert PRO diffractometer in Bragg–Brentano geometry, equipped with a secondary monochromator (Cu Kα radiation, $\lambda = 1.5418$ Å) and a X'Celerator detector.

2.3. In situ time resolved synchrotron powder X-ray diffraction (SR-PXD) and Rietveld refinement

In situ time resolved SR-PXD were collected at the Materials Science Beamline of the Swiss Light Source (SLS) at PSI Villigen, Switzerland. A glass capillary (o.d. 0.8 or 0.9 mm) containing the sample was heated from 303 to 512 K at a rate of 1, 4 or 20 K min^{-1}, while powder diffraction data were collected at temperature steps of 1, 4 and 8 K, respectively. The capillary was spun during exposure to the X-ray beam. Temperature was controlled with a STOE high temperature attachment, and data were

collected with a MYTHEN-II silicon strip detector at a wavelength of $\lambda = 0.7296$ Å, as calibrated by an external silicon standard. The SR-PXD data were refined using the Rietveld method and the program FULLPROF [35]. The structural model of trigonal $Mn(BH_4)_2$ [31] was used as starting model for the solid solution $Mg_xMn_{(1-x)}(BH_4)_2$. Magnesium was allowed to occupy two available sites in the $Mn(BH_4)_2$ model together with manganese. The atomic coordinates were fixed at the values given in Černý et al. [31]. Only one common isotropic displacement parameter was refined, in addition to the lattice parameters and peak shapes, which were modeled with pseudo-Voigt functions. The same refinement strategy was applied to α-$Mg(BH_4)_2$ when present in the sample (structural model from Filinchuk et al. [30]). However, here cation sites were constrained to be exclusively occupied by magnesium.

2.4. Infrared (IR) spectroscopy of as-prepared samples

IR spectra were measured using a Bio-Rad Excalibur instrument equipped with a Specac low temperature Golden Gate diamond attenuated total reflection (ATR) infrared spectroscopy system. The spectral resolution was set to 1 or 2 cm^{-1} for the different experiments. Samples were loaded into the ATR system in a glove box.

2.5. Thermogravimetry (TG), in situ Fourier transform infrared (FTIR) spectroscopy and mass spectrometry (MS)

TG–FTIR–MS measurements were performed with a TG Setsys "Evo" apparatus from Setaram Instrumentation coupled on-line to a FTIR Thermo Nicolet 380 spectrometer as well as to a MS Pfeiffer Omnistar spectrometer (corrosive gas version). In all experiments the carrier gas used was argon (Air Liquide Alphagaz 1, with a purity of $O_2 < 2$ p.p.m., $H_2O < 3$ p.p.m. and total hydrocarbon (C_xH_y) < 0.5 p.p.m.) at a flow of 100 ml min^{-1}. Heating was carried out at a rate of 5 K min^{-1} and a corundum crucible was used as the sample holder. The advantage of using both TG–MS and TG–FTIR is unambiguous interpretation of the results obtained with volatile products.

The TG–MS experiments were performed by coupling a thermobalance to a quadrupole mass analyzer (1–200 a.m.u. mass range) using a temperature controlled gas transfer line with a stainless steel capillary. During detection of the evolved species the turbo molecular pump is protected against corrosion and formation of an explosive gas mixture by a continuous flow of argon. The targeted fragments H_2 ($m/z = 2$) and B_2H_6 ($m/z = 27$) were monitored vs. temperature in multiple ion detection mode.

The TG–FTIR results were obtained using a stainless steel cell equipped with a BaF_2 optical window which allows species detection in the range of 4400–740 cm^{-1}. Decomposition gasses are passed through a temperature gas transfer line equipped with a perfluoroalkoxy capillary. Both the gas sample cell and the gas transfer line are maintained at a constant temperature of 443 K to avoid cold heat sinks and thus prevent condensation of the evolved gases. The chemigrams 1660–1520 and 1178–1168 cm^{-1}, indicating the presence of B_2H_6 in the gas stream released from the sample, were monitored vs. temperature. The spectra were collected at a resolution of 2 cm^{-1}, with 32 scans being summed for each spectrum.

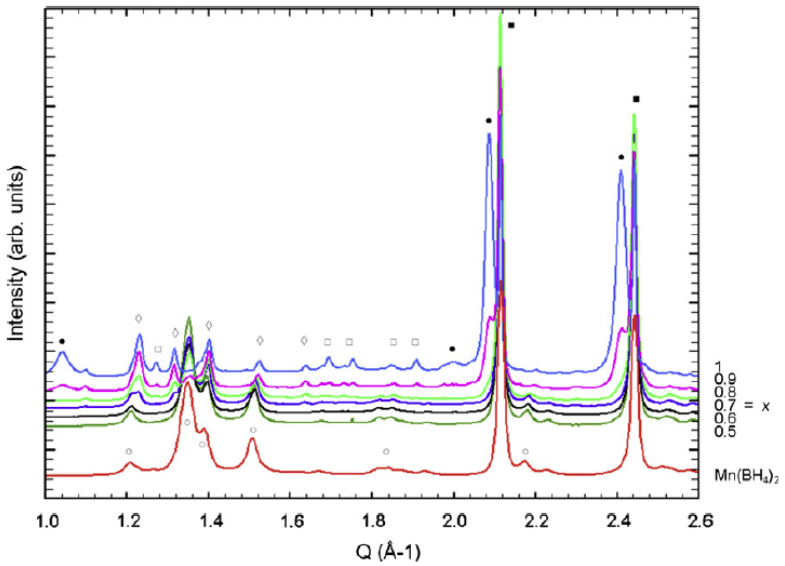

Fig. 1. The SR-PXD powder patterns of the ball milled mixtures $xMgCl_2 + (1\_x)MnCl_2 + 2LiBH_4$ at room temperature. The powder pattern of pure $Mn(BH_4)_2$ was measured on the sample from Černý et al. [31]. The units on the horizontal axis are $Q = 4\pi \sin(\theta)/\lambda$ (Å^{-1}). ●, Li_2MgCl_4; ■, LiCl; ○, $Mn(BH_4)_2$; □, RT-$LiBH_4$; ◇, $Mg(BH_4)_2$.

2.6. Inductively coupled plasma atomic emission spectroscopy (ICP-AES) of desorbed samples

The desorption products of two different representative compositions, pure $Mn(BH_4)_2$ and a solid solution with $x = 0.5$ (Eq. (1)), were studied by inductively coupled plasma atomic emission spectroscopy (ICP-AES) in order to trace any potential changes regarding the molar ratios between B and other detectable atoms (Li, Mg, and Mn), which in turn would suggest that the sample may be desorbing diborane B_2H_6. The elemental analysis was performed after complete dissolution of the powder sample in a hydrochloric acid solution using a Varian 720-ES optical emission spectrometer.

3. Results and discussion

3.1. Phase composition from the Rietveld refinement

The room temperature powder patterns of the ball milled mixtures are compared in Fig. 1. Phases of the solid solution series $Mg_xMn_{(1-x)}(BH_4)_2$ are formed in all mixtures, with exception of the manganese-free sample. $Mg_xMn_{(1-x)}(BH_4)_2$ crystallizes in the trigonal structure type of $Mn(BH_4)_2$. For nominal compositions with $x > 0.7$ α-$Mg(BH_4)_2$ is additionally formed.

The refined phase composition of the different ball milled mixtures is given in Table 1. The Rietveld plots are shown in Supplementary Information, Figs. S1–S6.

When, in the following discussions, we refer simultaneously to the chlorides and borohydrides of both magnesium and manganese cations we will describe them as MCl_2 and $M(BH_4)_2$, respectively. For $x = 0.5$–0.7 the ball milling reaction may then be written as:

$$MCl_2 + 2LiBH_4 \rightarrow M(BH_4)_2 + 2LiCl \quad (2)$$

Increasing the Mg fraction to $x = 0.8$–1 results in the formation of the ternary chloride Li_2MgCl_4 as an impurity. One may also expect Mg/Mn mixing to a certain extent in this phase, however, close inspection of its cubic lattice parameter $a = 10.4132(2)$ Å reveals that it is in good agreement with the values for the Mn-free end member found in the literature, i.e. $a = 10.417(1)$ Å for Li_2MgCl_4 [36], while $a = 10.4940(2)$ Å for Li_2MnCl_4 [37]. The thermal evolution of the cubic lattice parameter of Li_2MgCl_4 alone (see Supplementary Information, Fig. S7) does not allow us to exclude the dissolution of residual Mn in the ternary chloride at higher temperatures. The ball milling reaction can then be written as:

$$2MCl_2 + 4LiBH_4 \rightarrow M(BH_4)_2 + Li_2MgCl_4 + 2LiBH_4 \quad (3)$$

which is followed by a not fully completed reaction (Li_2MgCl_4 and $LiBH_4$ are still observed in the sample):

$$Li_2MgCl_4 + 2LiBH_4 \leftrightarrow 4LiCl + Mg(BH_4)_2 \quad (4)$$

as proposed in Chłopek et al. [38]. The fact that part of the magnesium is fixed in Li_2MgCl_4, as follows from Eq. (3), accounts for the lower refined magnesium concentration in $M(BH_4)_2$ for $x = 0.9$. The reaction during ball milling can also be written as:

$$MCl_2 + 2LiBH_4 \rightarrow M(BH_4)_2 + 2LiCl \quad (5)$$

with a parallel reaction taking place as:

$$2LiCl + MgCl_2 \rightarrow Li_2MgCl_4 \quad (6)$$

which is also in agreement with the phase analysis by Rietveld refinement (Table 1). This is due to the fact that less $MgCl_2$ is available as Eq. (6) proceeds, which in turn adversley affects Eq. (5) and thus results in unreacted $LiBH_4$.

The refined phase composition yields a deficit of trigonal $Mg_xMn_{(1-x)}(BH_4)_2$ for samples with nominal compositions $x = 0.5$–0.7. This may be explained by the formation of Li_2MgCl_4 at the above stated nominal compositions, but as an amorphous phase.

According to Chłopek et al. [38] Eq. (4) produces $Mg(BH_4)_2$ crystallizing in a structure type different from hexagonal α-$Mg(BH_4)_2$. Indeed, judging from Fig. 3 in Chłopek et al. [38] we can conclude that the crystalline form of $Mg(BH_4)_2$ produced by long ball milling (80 h) is very likely that of trigonal $Mn(BH_4)_2$.

3.2. Magnesium/manganese solid solution borohydride

The unit cell volume V of the trigonal solid solution borohydride $Mg_xMn_{(1-x)}(BH_4)_2$ decreases as the Mg content is increased (Fig. 2), undoubtedly owing to the difference in ionic radii between tetrahedrally coordinated Mg^{2+} (0.71 Å) and Mn^{2+} (0.80 Å), assuming the literature values in Shannon [39]. Interestingly, the lattice parameters of

Table 1
Phase composition of the ball milled mixtures $xMgCl_2 + (1 - x)MnCl_2 + 2LiBH_4$ from Rietveld refinement.

Nominal magnesium content x	Refined magnesium content x	$Mg_xMn_{(1-x)}(BH_4)_2$ (mol.%)	LiCl (mol.%)	Li_2MgCl_4 (mol.%)	α-$Mg(BH_4)_2$ (mol.%)	$LiBH_4$ (mol.%)
0.5	0.481(7)	0.172(2)	0.828(2)			
0.6	0.691(2)	0.202(3)	0.798(3)			
0.7	0.69(1)	0.136(2)	0.795(3)	–	0.069(1)	
0.8	0.84(2)	0.100(3)	0.732(3)	0.007(1)	0.124(1)	0.036(1)
0.9	0.82(8)	0.028(3)	0.513(2)	0.076(1)	0.269(4)	0.114(5)
1.0			0.168(2)	0.191(1)	0.243(2)	0.398(6)

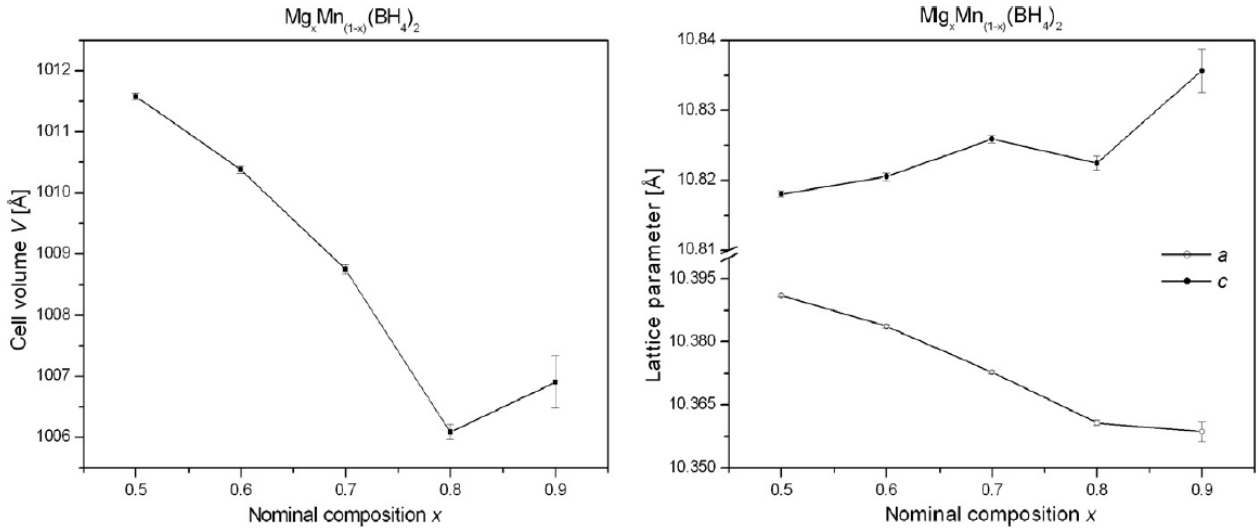

Fig. 2. Cell volume (left) and lattice parameters (right) as a function of nominal magnesium content in the trigonal $Mg_xMn_{(1-x)}(BH_4)_2$.

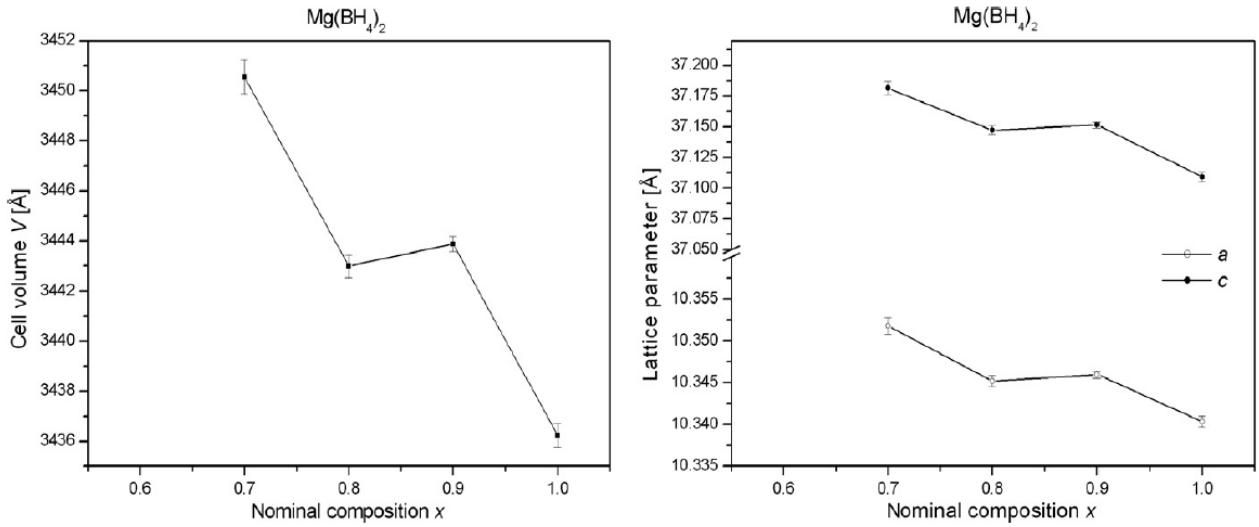

Fig. 3. Cell volume (left) and lattice parameters (right) as a function of nominal magnesium content in the hexagonal $Mg(BH_4)_2$.

$Mg_xMn_{(1-x)}(BH_4)_2$ respond anisotropically to substitution on the cation site, a increasing and c decreasing as a function of Mg content.

The refined magnesium content x in trigonal $Mg_xMn_{(1-x)}(BH_4)_2$ is given in Table 1. The upper limit of magnesium solubility is ~0.8, which stands somewhat in contradiction of the appearance of $Mg(BH_4)_2$ at the lower value of $x = 0.7$. The ball milling synthesis, which is not necessarily performed under equilibrium conditions, may be the origin of this discrepancy. Concerning chemical substitution on the cation site our refinements reveal that magnesium shows a preference for the higher symmetrical $M2$ site [31] in the trigonal solid solution borohydride. At $x = 0.8$ this site is exclusively occupied by Mg (Supplementary information, Table S1), while on $M1$, the other available site, Mg reaches its maximum occupancy value of 76% at $x = 0.8$.

The same dependency of cell volume V on Mg content is also reflected in the behavior of hexagonal α-$Mg(BH_4)_2$, V decreasing as the Mg content increases (Fig. 3). However, in contrast to the above results, the lattice parameters a and c behave isotropically in this case, and for $x = 1$ they agree well with the values reported in the literature [30]. The minor amount of α-$Mg(BH_4)_2$ phase in the samples and its complex structure prevented us from obtaining reliable refinements with respect to Mn solubility in the structure of hexagonal α-$Mg(BH_4)_2$. Nevertheless, judging from the comparison of the a-lattice parameter between α-$Mg(BH_4)_2$ and pure $Mn(BH_4)_2$ and from the phase

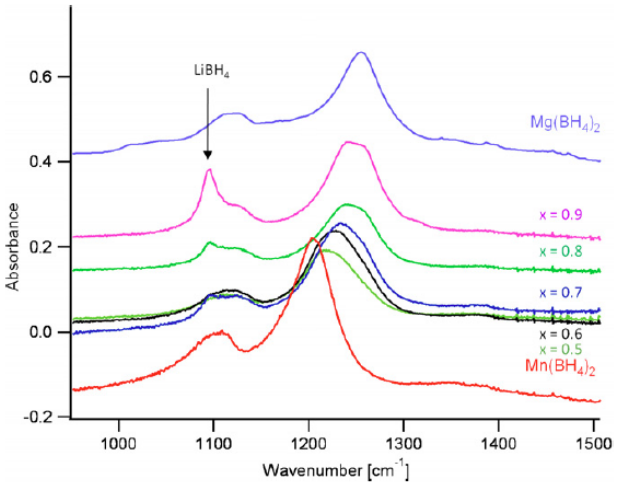

Fig. 4. The IR spectra of ball milled mixtures $x\mathrm{MgCl_2} + (1-x)\mathrm{MnCl_2} + 2\mathrm{LiBH_4}$. The IR spectra of pure $\mathrm{Mg(BH_4)_2}$ and $\mathrm{Mn(BH_4)_2}$ were collected on samples from Filinchuk et al. [30] and Černý et al. [31], respectively. Starting from $x = 0.7$ the $\mathrm{LiBH_4}$ peak appears at $\sim$1090 $\mathrm{cm^{-1}}$. Note that Rietveld refinement can quantify the $\mathrm{LiBH_4}$ content only starting from $x = 0.8$.

composition at different nominal compositions (Table 1) we can conclude that it does not exceed 10 mol.%.

3.3. Infrared spectroscopy

The IR spectra of the ball milled mixtures are shown in Fig. 4. The spectrum of pure $\mathrm{Mn(BH_4)_2}$ shows only two peaks, at 1100 and 1200 $\mathrm{cm^{-1}}$, in agreement with Černý et al. [31]. Increasing the magnesium content causes splitting of the band at 1100 $\mathrm{cm^{-1}}$, as observed for pure α-$\mathrm{Mg(BH_4)_2}$ [30]. Starting from $x = 0.7$, the peak related to $\mathrm{LiBH_4}$ appears at $\sim$1090 $\mathrm{cm^{-1}}$. The band above 1200 $\mathrm{cm^{-1}}$ is clearly composed of two similar peaks indicating the presence of two distinct cations in the trigonal $\mathrm{Mg_xMn_{(1-x)}(BH_4)_2}$ solid solution, as well as the presence of the second phase hexagonal α-$\mathrm{Mg(BH_4)_2}$ at higher magnesium contents. Generally the effect of substitution manifests itself in the shift of all vibrational bands to higher frequencies (higher wavenumber) with increasing magnesium content, obviously due to the difference in atomic mass between Mg and Mn.

3.4. Thermal decomposition by in situ SR-PXD

The results obtained from the in situ thermal decomposition SR-PXD experiments show that the diffraction peaks of the solid solution borohydride $\mathrm{Mg_xMn_{(1-x)}(BH_4)_2}$ disappear between 425 and 450 K. These values agree well with those found for pure $\mathrm{Mn(BH_4)_2}$ [31], however, as opposed to the structural analysis, a clear dependency on magnesium content x cannot be established here. From the TG experiments (see below) it follows that this temperature corresponds to gas release from the samples. However, the intensity of the $\mathrm{Mg_xMn_{(1-x)}(BH_4)_2}$ diffraction peaks starts to decrease already at 313 K. Surprisingly, the cell volume V also starts to decrease at that temperature. A similar behavior has been reported for pure $\mathrm{Mn(BH_4)_2}$ [31]. This suggests that the trigonal structure is already unstable close to room temperature, but subject to very slow decomposition kinetics. Annealing a sample

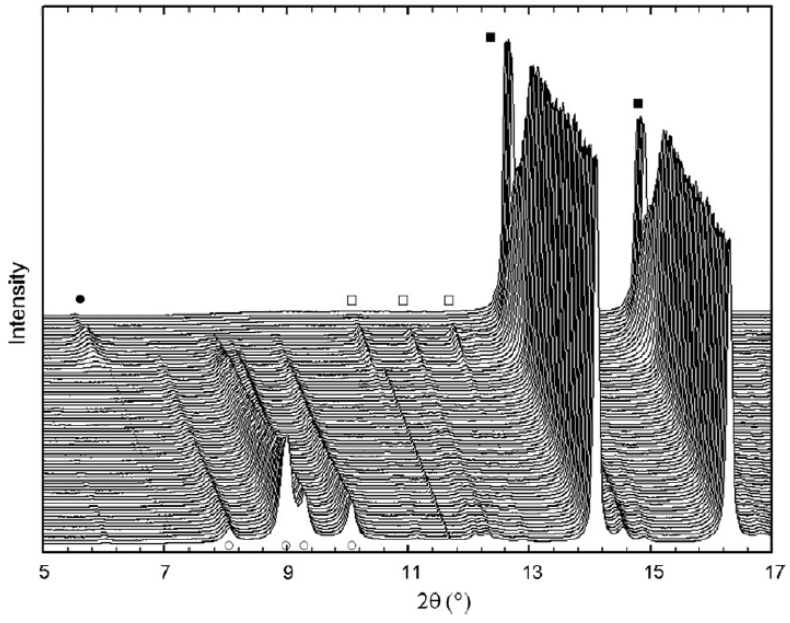

Fig. 5. Temperature ramp (powder patterns as a function of the temperature) for $\mathrm{Mg_{0.5}Mn_{0.5}(BH_4)_2}$ between 305 (bottom) and 512 (top) K. Synchrotron radiation, $\lambda = 0.7296$ Å. ●, $\mathrm{Li_2MgCl_4}$; ■, LiCl; ○, $\mathrm{Mg_{0.5}Mn_{0.5}(BH_4)_2}$; □, HT-$\mathrm{LiBH_4}$.

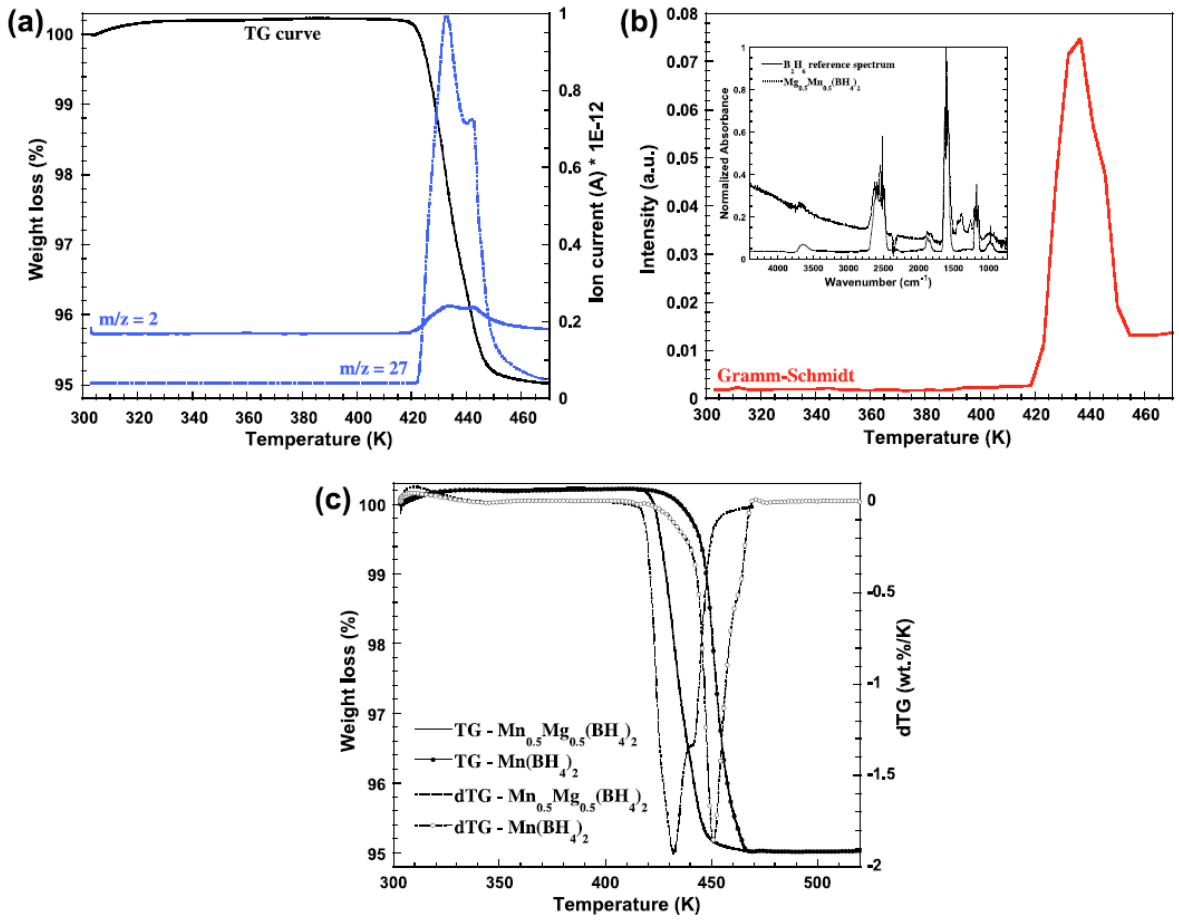

Fig. 6. Coupled TG and MS analysis of $Mg_{0.5}Mn_{0.5}(BH_4)_2$ monitoring fragments of H_2 ($m/z = 2$) and B_2H_6 ($m/z = 27$). (a) In situ FTIR analysis (Gramm-Schmidt) of the thermal decomposition of $Mg_{0.5}Mn_{0.5}(BH_4)_2$ with the observed and standard B_2H_6 FTIR spectra in the inset (b), and (c) TG results for $Mn(BH_4)_2$ and $Mg_{0.5}Mn_{0.5}(BH_4)_2$.

of $Mg_xMn_{(1-x)}(BH_4)_2$ with $x = 0.8$ at 360 K for 8 h results in complete disappearance of all Bragg signals belonging to this phase, which is in perfect agreement with the results of Varin and Zbroniec [40]. On the other hand, the samples are stable for several months when stored under an argon atmosphere at room temperature.

When hexagonal α-$Mg(BH_4)_2$ is present in the sample its diffraction peaks vanish simultaneously with those pertaining to $Mg_xMn_{(1-x)}(BH_4)_2$, i.e. before the transformation to β-$Mg(BH_4)_2$, which is reported to occur at 458 [28,41] or 490 K [30], and at a much lower temperature than the decomposition of β-$Mg(BH_4)_2$, reported to occur at 518 [41] or 548 K [42]. The eutectic relation with $LiBH_4$ in the sample is at the origin of α-$Mg(BH_4)_2$ melting, as was observed recently [43]. Room temperature $LiBH_4$ transforms to high temperature $LiBH_4$ at 381 K, in agreement with Filinchuk et al. [44] and Mauron et al. [45].

Above 393 K we can observe an increase in the intensity of diffraction peaks arising from $LiBH_4$ and Li_2MgCl_4 in all samples except for $x = 1$, which was not studied by in situ SR-PXD. This intensity gain is in turn accompanied by a decrease in signals arising from LiCl (Fig. 5). This can be accounted for by Eq. (4) taking place in the opposite direction, which does not proceed below 360 K, as follows from sample $x = 0.8$, which was annealed at precisely that temperature for 8 h. Even after long annealing no diffraction peaks of $LiBH_4$ and Li_2MgCl_4 were observed. Independent of the degree of Mg substitution x (with exception of $x = 1$), the diffraction peaks of Li_2MgCl_4 start to disappear between ~493 and 512 K, together with the peaks of high temperature $LiBH_4$. Simultaneously, the intensity of the LiCl peaks again increases (Fig. 5). This indicates that Eq. (4) now proceeds from left to the right, and occurs below the $LiBH_4$ melting point of 541 K [45].

Reactions similar to Eq. (4) have also been observed for other transition metals. In $ZnCl_2 + ABH_4$ (A = Li or Na) mixtures A_2ZnCl_4 reacts with ABH_4 in analogy to Eq. (4), but only at higher temperatures (~430 K), and the reaction products are metallic Zn and ACl involving hydrogen and diborane release [20]. For $ScCl_3 + ABH_4$ (A = Na or K) mixtures a similar reaction between K_3ScCl_6 and ABH_4 takes place for A = K at 500 K [19], while for A = Na reaction between Na_3ScCl_6 and melted $Na(ScBH_4)_4$ is observed at 430 K [18], involving formation of NaCl.

3.5. Thermal decomposition by TG, in situ FTIR spectroscopy and MS

The results of the coupled TG and MS analysis of $Mg_{0.5}Mn_{0.5}(BH_4)_2$ monitoring the fragments H_2 ($m/z = 2$) and B_2H_6 ($m/z = 27$) are shown in Fig. 6a, while the findings of the in situ FTIR analysis (Gramm–Schmidt curve representative of the total absorbance intensity) of the thermal decomposition of $Mg_{0.5}Mn_{0.5}(BH_4)_2$ are presented in Fig. 6b. The reference data for pure $Mn(BH_4)_2$ obtained from the same analysis are given in Supplementary Information Fig. S8a and b, with the chemigrams of both samples shown in Fig. S9a and b.

In both cases the TG analyses of $Mg_{0.5}Mn_{0.5}(BH_4)_2$ and $Mn(BH_4)_2$ samples provide a weight loss of 5.20% (Fig. 6c). The first derivative of the TG curve shows the main peak emerging at 433 K for $Mg_{0.5}Mn_{0.5}(BH_4)_2$ and at 453 K for $Mn(BH_4)_2$, in good agreement with our SR-PXD data. A second peak is observed a few Kelvin higher for both samples, and alludes to the complex decomposition process, including intermediate phases, reported recently [46,47]. Mass spectroscopy shows that the desorbed gas contains diborane and hydrogen (Figs. 6a and S8a). Diborane is quite stable at room temperature without the presence of catalysts, but starts to decompose rapidly above 473 K [48]. The presence of diborane in desorbed gases from both samples is confirmed by the in situ FTIR data (Figs. 6b and S8b), which agree very well with the findings from TG and MS; thus the double desorption event is observed by all three techniques. The insets in Figs. 6b and S8b show the FTIR spectra measured at the Gramm–Schmidt peak compared with the reference data for B_2H_6 (gas) reported in the NIST Chemistry Webbook (http://webbook.nist.gov/chemistry/). The matching is good, nevertheless, we can observe some differences (extra peaks): (i) in the range 2400–2300 cm^{-1} a doublet can be assigned to residual CO_2 (ν C=O 2345 cm^{-1}); (ii) in the range 1500–1200 cm^{-1}, three peaks can be assigned to B_5H_9 [49], a pyrolytic decomposition product of diborane.

The weight losses observed by TG are also in agreement with the presence of diborane in the desorbed gas. Using the molar fractions from the Rietveld analysis (Table 1) the weight losses can be explained (see Supplementary Information, Table S2) by the reaction:

$$M(BH_4)_2 \rightarrow yB_2H_6(gas) + (4-3y)H_2(gas) + M + (2-2y)B \quad (7)$$

with $y = 0.26$ for $Mg_{0.5}Mn_{0.5}(BH_4)_2$ and $y = 0.11$ for $Mn(BH_4)_2$ samples. This means that the desorbed gas contains 92.5–97 mol.% hydrogen and 7.5–3 mol.% diborane.

The room temperature PXD data of both desorbed samples show LiCl and Li_2MgCl_4 as crystalline phases, the latter occurring only in the sample with $x = 0.5$ (see Supplementary Information, Figs. S10 and S11). The cubic lattice parameter $a = 10.46$ Å of Li_2MgCl_4 indicates the dissolution of a small amount of Mn in the ternary chloride. The strong amorphous signal in the powder patterns of the desorbed samples is caused by to the Scotch tape used to fix the small quantity of available powder. The in situ SR-PXD data for both samples (data for pure $Mn(BH_4)_2$ are from the Černý et al. [31], 3:1 mixture) were collected at the same temperature as the maximum temperature in the TG analysis (473 K) and confirm the observed phases, as well as revealing the presence of $LiBH_4$ produced by the reverse Eq. (4). This shows that not all hydrogen was desorbed in the in situ SR-PXD experiment at 473 K, in contrast to the TG experiment. The reason for this is undoubtedly the time spent at a given temperature, which is much shorter during the in situ SR-PXD experiment than in the TG analysis.

Quantitative analysis of the desorbed gases can also be extracted from the results obtained by MS, but the accuracy strongly depends on the selection of the standard sample. We therefore opted to verify the ratio between the desorbed diborane and hydrogen via chemical analysis of the desorbed samples by means of ICP-AES, which is a standard-free method. In the case of diborane desorption the molar ratio between B and other detectable species in the sample (Li, Mg, and Mn) would deviate from the nominal ratio. The results of the ICP-AES analysis are given in Supplementary Information Table S3. The ratio B/M lies within the range 2.03–2.15 for both as-synthesized samples, decreasing to 1.65 for $Mg_{0.5}Mn_{0.5}(BH_4)_2$ and to 1.76 for $Mn(BH_4)_2$, referring to desorbed samples. These results yield values of $y = 0.18$ and 0.12, respectively, with respect to Eq. (7), which is in good agreement with the TG experiment taking into account the higher uncertainty in the weight fraction of phases as estimated from Rietveld refinement for the $Mg_{0.5}Mn_{0.5}(BH_4)_2$ sample.

According to the inverse relation between the decomposition temperature of a metallic borohydride and the cation electronegativity [4,6] $Mg(BH_4)_2$ should decompose at a higher temperature than $Mn(BH_4)_2$ or even mixed $Mg_{0.5}Mn_{0.5}(BH_4)_2$ ($\chi_e = 1.31$ for Mg, $\chi_e = 1.55$ for Mn). Indeed, β-$Mg(BH_4)_2$ decomposes at 518 [41] or 548 K [42], which is higher than what is observed in this work for both $Mn(BH_4)_2$ (453 K) and $Mg_{0.5}Mn_{0.5}(BH_4)_2$ (433 K). On the other hand, the cation with higher electronegativity (Mn) seems to control the stability of the mixed borohydride $Mg_{0.5}Mn_{0.5}(BH_4)_2$, rather than the average electronegativity of both cations.

Thermal desorption of $MnCl_2 + 3LiBH_4$ mixtures was studied earlier [40,50] with the presumption of $LiMn(BH_4)_3$ formation [50]. However, from the published powder patterns therein (Fig. 3 in Choudhury et al. [50]) it seems that the studied samples in fact contain $Mn(BH_4)_2$ and excess $LiBH_4$ (besides LiCl), rather than the ternary compound. The endothermic peak at 371–372 K in the DSC signals (Figs. 4 and 5 in Choudhury et al. [50]) assigned to $LiMn(BH_4)_3$ melting should therefore be related to the room temperature–high temperature phase transformation of $LiBH_4$ (observed at 381 K [44,45]). Thermal desorption occurred between 416 and 438 K, depending on the heating

rate (2–20 K min^{-1}). It has, however, been observed after a few hours at 373 K [40]. Gas chromatography showed that the desorbed gas (temperature unknown) contained mostly hydrogen [50]. The weight losses corresponded to 3.75 H_2 below 473 K and to 6.5 H_2 above 723 K [40], where excess $LiBH_4$ certainly also desorbs (desorption observed at 703 K [45]). Surprisingly the weight loss corresponding to ~6.5 H_2 was already observed at 416 K [50].

4. Conclusions

The magnesium and manganese borohydrides form a solid solution with refined composition $Mg_xMn_{(1-x)}(BH_4)_2$ ($x = 0$–0.8) conserving the trigonal structure of $Mn(BH_4)_2$. Magnesium shows a preference for the higher symmetric site in the trigonal borohydride, which is exclusively occupied by Mg at $x = 0.8$. The second cation site can accommodate up to 75% of magnesium for $x = 0.8$. Manganese is also dissolved in the hexagonal structure of α-$Mg(BH_4)_2$, however with the upper solubility limit not exceeding 10 mol.%. A two phase region of trigonal and hexagonal borohydrides exists within the composition range $x_{Mg} = 0.8$–0.9.

The IR spectra show splitting of some peaks, indicating the presence of two cations in trigonal $Mg_xMn_{(1-x)}(BH_4)_2$ solid solutions, and also the presence of a second phase, hexagonal α-$Mg(BH_4)_2$, at higher magnesium contents. As the magnesium content increases all vibrational frequencies shift to higher wavenumbers.

The decomposition temperature of the trigonal $Mg_xMn_{(1-x)}(BH_4)_2$ ($x = 0$–0.8) does not vary significantly with magnesium content (433–453 K). The desorbed gas contains mostly hydrogen and 3–7.5 mol.% diborane B_2H_6, as is concluded from thermogravimetry, mass and infrared spectrometry, as well as atomic emission spectroscopy analyses of $Mn(BH_4)_2$ and $Mg_{0.5}Mn_{0.5}(BH_4)_2$ samples. This indicates that it is the cation with higher electronegativity (Mn) that controls the stability of the mixed borohydride $Mg_{0.5}Mn_{0.5}(BH_4)_2$, rather than the average electronegativity of both cations.

When hexagonal α-$Mg(BH_4)_2$ is present in the sample its diffraction peaks disappear simultaneously with the $Mg_xMn_{(1-x)}(BH_4)_2$ peaks, i.e. before its transformation to β-$Mg(BH_4)_2$, as a consequence of the eutectic relation with $LiBH_4$.

The solid solution $Mg_xMn_{(1-x)}(BH_4)_2$ is a promising material for hydrogen storage as it decomposes at a similar temperature to $Mn(BH_4)_2$, i.e. at a much lower temperature than pure $Mg(BH_4)_2$, without significantly losing hydrogen weight capacity, thanks to the substitution of Mn by Mg up to 80 mol.%. Diborane release and the same question as for the pure $Mg(BH_4)_2$, reversibility, remain to be addressed.

Acknowledgements

This work was supported by the Swiss National Science Foundation. The authors acknowledge SLS for the beamtime allocation, F. Gozzo (SLS) for help with the data collection, and P. Schouwink (University of Geneva) for careful reading of the manuscript.

Appendix A. Supplementary material

Supplementary data associated with this article can be found, in the online version, at doi:10.1016/j.actamat.2011.04.052.

References

[1] Soloveichik G. Mater Matters 2007;2:11–4.
[2] Orimo S, Nakamori Y, Eliseo JR, Züttel A, Jensen CM. Chem Rev 2007;107:4111–32.
[3] Grochala W, Edwards PP. Chem Rev 2004;104:1283–315.
[4] Schrauzer GN. Naturwissenschaften 1995;42:438.
[5] Miwa K, Ohba N, Towata S, Nakamori Y, Orimo S. J Alloys Compd 2005;404–406:140–3.
[6] Nakamori Y, Miwa K, Ninomiya A, Li H-W, Ohba N, Towata S, et al. Phys Rev B 2006;74:045126.
[7] Li H-W, Orimo S, Nakamori Y, Miwa K, Ohba N, Towata S, et al. J Alloys Compd 2007;446–447:315–8.
[8] Nakamori Y, Orimo S. J Alloys Compd 2004;370:271–5.
[9] Zhang J, Černý R, Villeroy B, Godart C, Chandra D, Latroche M. J Alloys Compd, in press, DOI: 10.1016/j.jallcom.2010.09.160.
[10] Filinchuk Y, Chernyshov D, Dmitriev V. In: Demirci UB, Miele P, editors. Boron hydrides, high potential hydrogen storage material. Hauppauge, NY: Nova Publishers; 2010.
[11] Filinchuk Y, Chernyshov D, Dmitriev V. Z Kristallogr 2008;223:649–59.
[12] Nakamori Y, Orimo S. In: Walker G, editor. Solid-state hydrogen storage, materials and chemistry. Abington: Woodhead Publishing; 2008. p. 420–49.
[13] Kim Ch, Hwang SJ, Bowman Jr RC, Reiter JW, Zan JA, Kulleck JG, et al. J Phys Chem C 2009;113:9956–68.
[14] Nöth H, Wiberg E, Winter LP. Z Anorg Allg Chem 1971;386:73–86.
[15] Hagenmuller P, Rault M. Compt. Rendu Acad. Sci. 1959;248:2758–60.
[16] Hummelshøj JS et al. J Chem Phys 2009;131:014101.
[17] Hagemann H, Longhini M, Kaminski JW, Wesolowski TA, Černý R, Penin N, et al. J Phys Chem A 2008;112:7551–5.
[18] Černý R, Severa G, Ravnsbæk D, Filinchuk Y, D'Anna V, Hagemann H, et al. J Phys Chem C 2010;114:1357–64.
[19] Černý R, Ravnsbæk D, Severa G, Filinchuk Y, D'Anna V, Hagemann H, et al. J Phys Chem C 2010;114:19540–9.
[20] Ravnsbæk D, Filinchuk Y, Cerenius Y, Jakobsen HJ, Besenbacher F, Skibsted J, et al. Angew Chem Int Ed 2009;48:6659–63.
[21] Lindemann I, Domènech Ferrer R, Dunsch L, Filinchuk Y, Černý R, Hagemann H, et al. Chem Eur J 2010;16:8707–12.
[22] Lindemann I, Domènech Ferrer R, Dunsch L, Černý R, Hagemann H, D'Anna V. et al., Faraday Discus, in press. doi:10.1039/c0fd000d4h.
[23] Keiderling TA, Wozniak WT, Gay RS, Jurkowitz D, Bernstein ER, Lippard SJ, et al. Inorg Chem 1975;14:576.
[24] Mosegaard L, Møller B, Jørgensen J-E, Filinchuk Y, Cerenius Y, Hanson J, et al. J Phys Chem C 2008;112:1299–303.
[25] Ravnsbæk D, Sørensen LH, Filinchuk Y, Reed D, Book D, Cerenius Y, et al. Eur J Inorg Chem 2010;11:1608–12.
[26] Kedrova NS, Mal'tseva NN. Zhurnal Neorganicheskoi Khmimii 1977;22:1791–4.
[27] Černý R, Filinchuk Y, Hagemann H, Yvon K. Angew Chem Int Ed 2007;46:5765–7.
[28] Her J-H, Stephens PW, Gao Y, Soloveichik GL, Rijssenbeek J, Andrus M, et al. Acta Crystallogr B 2007;63:561–8.
[29] Dai B, Sholl DS, Johnson JK. J Phys Chem C 2008;112:4391–5.

[30] Filinchuk Y, Černý R, Hagemann H. Chem Mater 2009;21(5):925–33.
[31] Černý R, Penin N, Hagemann H, Filinchuk Y. J Phys Chem C 2009;113:9003–7.
[32] Portier J, Tressaud A, Menil F, Claverie J, De Pape R, Hagenmuller P. J Sol State Chem 1969;1:100–2.
[33] Okada O. J Phys Soc Jpn 1982;48:391–8.
[34] Hagemann H, Černý R. Dalton Trans 2010;39:6006–12.
[35] Rodriguez-Carvajal J. Physica B 1993;192:55–69.
[36] Wickel C, Lutz HD. Z Kristallogr 1998;213:27.
[37] Wickel C, Zhang Z, Lutz HD. Z Anorg Allg Chem 1994;620:1537–42.
[38] Chłopek K, Frommen C, Leon A, Zabara O, Fichtner M. J Mater Chem 2007;17:3496.
[39] Shannon RD. Acta Cryst. 1976;A32:751–67.
[40] Varin RA, Zbroniec L. Int J Hydrogen Energy 2010;35:3588–97.
[41] Riktor MD, Sørby MH, Chłopek K, Fichtner M, Buchter F, Züttel A, et al. J Mater Chem 2007;17:4939–42.
[42] Soloveichik GL, Gao Y, Rijssenbeek J, Andrus M, Kniajanski S, Bowman Jr RC, et al. Int J Hydrogen Energy 2009;34:916–28.
[43] Hagemann H, D'Anna V, Rapin JP, Černý R, Filinchuk Y, Ki Chul K, Sholl DS, Parker SF. J Alloys Compd, in press. doi:10.1016/j.jallcom.2010.10.068.
[44] Filinchuk Y, Chernyshov D, Černý R. J Phys Chem C 2008;112:10579–84.
[45] Mauron P, Buchter F, Friedrichs O, Remhof A, Bielmann M, Zwicky CN, et al. J Phys Chem. B 2008;112(3):906–10.
[46] Van Setten MJ, Lohstroh W, Fichtner M. J Mater Chem 2009;19:7081–7.
[47] Yang J, Zhang X, Zheng J, Song P, Li X. Scripta Mater 2011;64:225–8.
[48] Söderlund M, Mäki-Arvela P, Eränen K, Salmi T, Rahkola R, Murzin DYu. Catal Lett 2005;105:191–202.
[49] Hrostowski HJ, Pimentel GC. J Am Chem Soc 1954;76:998–1003.
[50] Choudhury P, Srinivasan SS, Bhethanabotla VR, Goswami Y, McGrath K, Stefanakos EK. Int J Hydrogen Energy 2009;34:6325–34.